

# FDRP Journal's

## IJSREAT-0000958

 16 FDRP IJSREAT

---

### Document Details

**Submission ID**

tm:oid:::1:3200238796

**Submission Date**

Mar 31, 2025, 1:27 PM GMT+7

**Download Date**

Mar 31, 2025, 1:28 PM GMT+7

**File Name**

IJSREAT-0000958.docx

**File Size**

755.2 KB

**13 Pages****3,300 Words****18,683 Characters**





# 10% Overall Similarity

The combined total of all matches, including overlapping sources, for each database.




## Filtered from the Report

- Bibliography
- Quoted Text

## Match Groups

-  **33** Not Cited or Quoted 9%  
Matches with neither in-text citation nor quotation marks
-  **3** Missing Quotations 1%  
Matches that are still very similar to source material
-  **0** Missing Citation 0%  
Matches that have quotation marks, but no in-text citation
-  **0** Cited and Quoted 0%  
Matches with in-text citation present, but no quotation marks

## Top Sources

- 5%  Internet sources
- 7%  Publications
- 1%  Submitted works (Student Papers)

## Match Groups

- 33** Not Cited or Quoted 9%  
Matches with neither in-text citation nor quotation marks
- 3** Missing Quotations 1%  
Matches that are still very similar to source material
- 0** Missing Citation 0%  
Matches that have quotation marks, but no in-text citation
- 0** Cited and Quoted 0%  
Matches with in-text citation present, but no quotation marks

## Top Sources

- 5% Internet sources
- 7% Publications
- 1% Submitted works (Student Papers)

## Top Sources

The sources with the highest number of matches within the submission. Overlapping sources will not be displayed.

<b>1</b>	Publication	<b>C. Guedes Soares, S. Wang. "Innovations in Renewable Energies Offshore", CRC Pr...</b>	<b>1%</b>
<b>2</b>	Internet	<b>www.mdpi.com</b>	<b>&lt;1%</b>
<b>3</b>	Student papers	<b>University of Wales Swansea</b>	<b>&lt;1%</b>
<b>4</b>	Student papers	<b>University of South Wales - Pontypridd and Cardiff</b>	<b>&lt;1%</b>
<b>5</b>	Internet	<b>www.cervicornconsulting.com</b>	<b>&lt;1%</b>
<b>6</b>	Publication	<b>A. Apparao, G. Chandra Sekhar. "Hybrid MDA-ANFIS approach based control of gri...</b>	<b>&lt;1%</b>
<b>7</b>	Student papers	<b>AlHussein Technical University</b>	<b>&lt;1%</b>
<b>8</b>	Internet	<b>ebin.pub</b>	<b>&lt;1%</b>
<b>9</b>	Internet	<b>hal.archives-ouvertes.fr</b>	<b>&lt;1%</b>
<b>10</b>	Publication	<b>S. Kiran Kumar Reddy, Harish Gupta, Vamshi Krishna Gandla, D. Venkat Reddy, Ra...</b>	<b>&lt;1%</b>

11	Publication	Singh, B, and S Sharma. "PMBLDCG based stand-alone wind energy conversion sy...	<1%
12	Internet	link.springer.com	<1%
13	Internet	www.tandfonline.com	<1%
14	Publication	Adel Merabet, Khandker Tawfique Ahmed, Hussein Ibrahim, Rachid Beguenane, ...	<1%
15	Publication	Ahmed, Tofael, Tey Soon, and Saad Mekhilef. "A Single Phase Doubly Grounded S...	<1%
16	Publication	Chayan Bhattacharjee, Binoy Krishna Roy. "Fuzzy-supervisory control of a hybrid ...	<1%
17	Publication	D. Kottick, M. Blau, D. Edelstein. "Battery energy storage for frequency regulation...	<1%
18	Publication	Habib Benbouhenni, Ilhami Colak, Mourad Yessef, Z.M.S. Elbarbary, Nicu Bizon. "F...	<1%
19	Publication	Kotb B. Tawfiq, Hatem Zeineldin, Ahmed Al-Durra, Ehab F. El-Sadaany. "Enhancing...	<1%
20	Publication	Zhang, Z., H. Xu, J. Zou, and G. Zheng. "Sliding Mode Control based Active Power C...	<1%
21	Internet	espace.etsmtl.ca	<1%
22	Internet	tel.archives-ouvertes.fr	<1%
23	Internet	trepo.tuni.fi	<1%
24	Internet	www.frontiersin.org	<1%

25	Internet	www.igi-global.com	<1%
26	Internet	www.ijirst.org	<1%
27	Publication	"Integration of Renewable Energy Sources with Smart Grid", Wiley, 2021	<1%
28	Publication	Benhalima Seghir, Ambrish Chandra, Rezkallah Miloud. "A New Control Strategy f...	<1%
29	Publication	Chung-Han Lin, Yuan-Kang Wu. "Overview of Frequency-Control Technologies for ...	<1%
30	Publication	N. Femia. "<![CDATA[Optimized one-cycle control in photovoltaic grid connected a...	<1%

# Comprehensive Performance Analysis of a Standalone Wind Energy System with Battery Storage and Optimized Inverter Control

D. Chandrashekar <sup>1</sup>, P. Satish Kumar <sup>2</sup>,

<sup>1</sup>Department of Electrical Engineering, Osmania University, Hyderabad.

<sup>2</sup>Department of Electrical Engineering, Osmania University, Hyderabad.

Corresponding Author: Chandrashekar@osmania.ac.in

**Abstract**-This paper explores a standalone renewable energy system that includes a wind generator and a battery energy storage (BES) module. The renewable source operates in parallel with the load, requiring synchronization control. Maximum power extraction from the wind generator is achieved using a sliding mode control perturb and observe (SMC P&O MPPT) technique, while the BES is linked to a common DC bus. An inverter employing active power control (APC) with an anti-windup proportional integral (AWPI) controller helps reduce harmonics. The system's performance is assessed by analyzing total harmonic distortion (THD) in inverter voltages and currents under optimized SMC MPPT and AWPI-based control strategies.

**Keywords:** PMBLDCG (Permanent Magnet Brushless DC generator), MPPT (Maximum Power Point Tracking), SMC P&O (Sliding Mode Control Perturb and Observe), APC (Active Power Control), AWPI Anti-windup Proportional Integral), – PI, Simulink.

## I. Introduction

The increasing cost of fossil fuels has accelerated the shift toward renewable energy sources, with wind energy being a highly efficient and environmentally sustainable option. Wind Energy Conversion Systems (WECS) rely on natural wind conditions, making power generation highly variable due to fluctuating meteorological factors. These inconsistencies create challenges for power grid stability and increase operational costs by requiring additional reserve capacity. To address these issues, accurate wind speed forecasting is essential, enabling grid operators to manage power fluctuations, optimize grid performance, and enhance wind energy integration.

Forecasting wind energy plays a vital role in maintaining grid balance, supporting power dispatch strategies, and aiding in electricity market operations. While wind power prediction is generally less accurate than load forecasting, advancements in forecasting models are continuously improving reliability. Various methods, including statistical models and machine learning algorithms, have been developed to enhance wind power prediction for better energy management.

The transition to renewable energy also highlights the need for energy storage solutions to address the intermittent nature of wind power. Battery Energy Storage Systems (BESS) play a crucial role in storing surplus energy when wind generation is high and supplying power during low-generation periods. This integration ensures a consistent power supply and improves overall system efficiency. By combining advanced forecasting techniques with energy storage solutions, wind energy can be more effectively utilized, reducing dependency on conventional power sources and contributing to a cleaner, more sustainable energy infrastructure [1].

The integration of renewable energy sources into the grid has become increasingly important as a means of replacing traditional power generation methods. These renewable sources are linked to the grid using various power electronic circuits to ensure consistent power supply. The grid may also operate as a microgrid, distributing power to local loads with lower

capacity. For effective grid integration, renewable sources must be synchronized with the grid's voltage magnitude, frequency, and phase angles. When connected to the main utility grid, these systems benefit from enhanced stability, as the grid serves as an infinite power source. In scenarios where renewable power generation is insufficient due to high load demand, the grid compensates for the shortfall. Conversely, when excess power is generated, it is fed back into the grid to support other network loads [2].

While grid-connected renewable systems offer greater reliability, standalone renewable systems pose challenges due to their unpredictable nature. Variations in power generation caused by fluctuations in natural energy sources make direct load connections impractical. To address this issue, energy storage systems, particularly battery energy storage (BES) modules, are used to store excess energy and supply power during periods of low generation. The BES is typically integrated at the DC link, where multiple modules, including renewable sources and loads, are connected. This configuration helps stabilize the DC link voltage and ensures a continuous power supply [3]. In this study, a standalone renewable energy system is analyzed, incorporating a wind energy generator and a BES to supply power to local loads.

## II. Wind Generation System

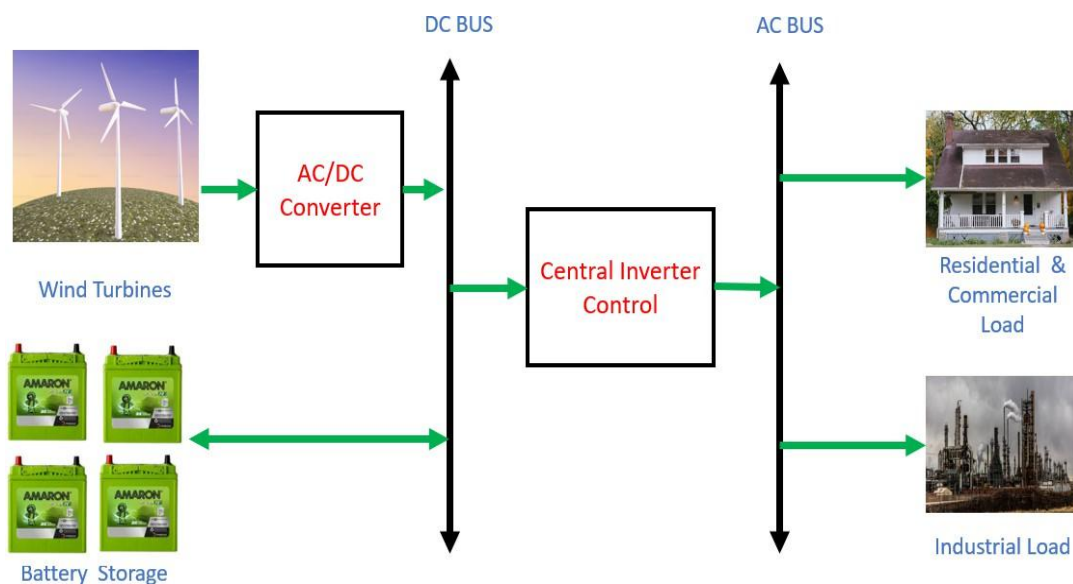


Figure 1: Standalone Wind Generation System

As per Figure 1 the overall schematic of the standalone renewable system has AC/DC converter for the wind turbines. BES is connected to the DC bus directly for power exchange [4]. These AC/DC converters of the renewable modules ensure maximum power extraction from wind generator. At the DC bus a central inverter and control is connected which converts DC power from the renewable and battery modules to AC. The converted AC is fed to residential and dump loads with controlled voltage and frequency controller.

The AC/DC converters are controlled by individual SMC P&O MPPT getting feedback signals from source voltage and current ( $V_{WT}$  and  $I_{WT}$ ). The central inverter is controlled by APC based AWPI control module with feedback signals from 3-ph load voltages and currents ( $V_{Labc}$  and  $I_{Labc}$ ) [5]. The interfacing inverter controller is the AWPI controller which reduced disturbances in the reference signals. This reduces the harmonics on the AC side of the inverter connected to the load. In this paper the standalone renewable source system outline diagram is discussed in section 1 which includes the description of integrated modules. The next section 2 has the circuit configuration of each module of the proposed renewable standalone system. For the wind generation conversion power is discussed in section 3. The new different proposed controllers is presented in section 4 with new inverter controller is discussed in section 5 has the results and analysis is discussed in section 6 conclusion and references of the paper determining the optimal controller for the standalone renewable

system.

### III. Proposed Advanced Controller for wind Generation System

As discussed earlier in Section 1, the proposed standalone renewable energy system consists of a wind generator. Additionally, battery energy storage devices are integrated at the DC link to maintain voltage stability [6]. A Permanent Magnet Brushless DC Generator (PMBLDCG) is utilized for power generation, receiving mechanical input torque from wind turbines driven by wind force. Since the system under consideration operates at a smaller scale, micro-turbines are employed to generate electricity. The complete system structure is illustrated in Figure 2.

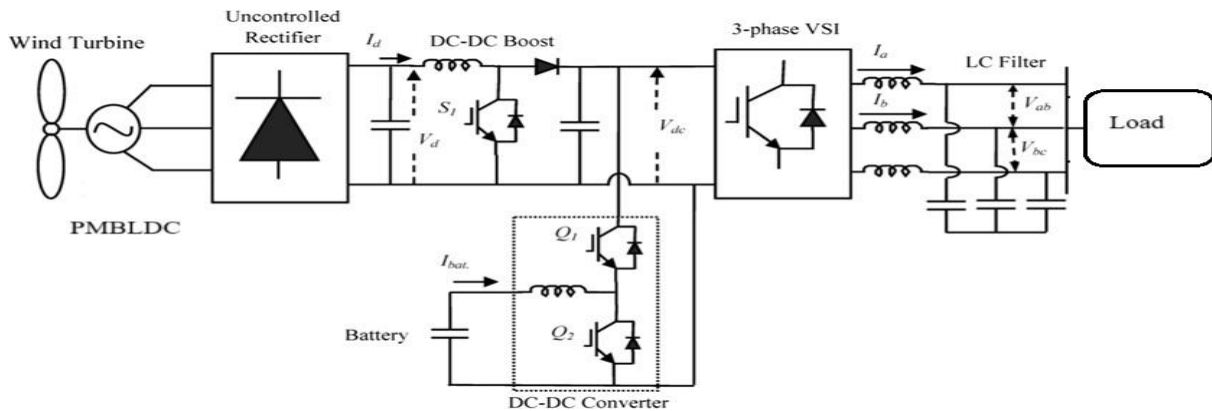


Figure 2: Circuit structure of wind renewable source system

As shown in Figure 2 the wind generator is integrated AC/DC is with single power IGBT switch each. As the PMBLDCG generates uncommuted voltage (trapezoidal AC voltage) a diode bridge rectifier (DBR) is connected to the machine terminals [7]. This DBR circuit converts the trapezoidal AC voltage to DC voltage which is taken as input to the boost converter. It is also observed that the battery pack is connected at the DC link which is directly connected to the interfacing DC/AC inverter [8]. For harmonic filtration a LC filter is connected between the load and the inverter designed as per the switching frequency and maximum load. There are the controllers for operating the power circuits of the renewable source and inverter. The controller for the wind generator is similar with only change in the input signals. The inverter controller is realized with feedback from load side measurement signals. A detailed structure of the proposed controllers and the expression for the design are explained below [9].

### IV. Sliding Mode Control Perturb and Observe MPPT (SMC P&O MPPT)

Among conventional Maximum Power Point Tracking (MPPT) techniques, the Perturb and Observe (P&O) method is widely used for optimizing power extraction from renewable energy sources. Every MPPT algorithm requires input voltage ( $V_{wt}$ ) and input current ( $I_{wt}$ ) as reference signals to determine either the reference voltage ( $V_{ref}$ ) or the duty cycle ( $D$ ). A method with a faster response to these input variations is generally considered more efficient. In this study, a modified P&O MPPT technique incorporating Sliding Mode Control (SMC) is implemented to regulate the Insulated Gate Bipolar Transistor (IGBT) switch in the AC/DC boost converter. The control structure of the proposed SMC P&O MPPT module, responsible for generating the duty ratio, is depicted in Figure 3.



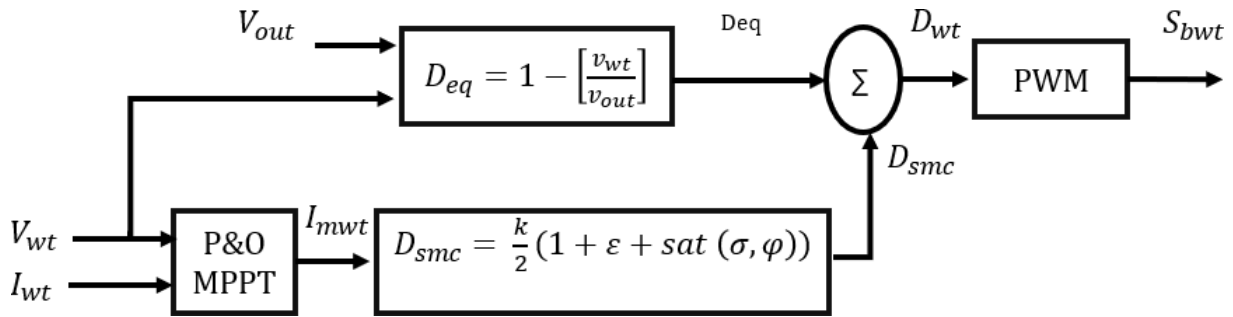


Figure 3: SMC P&O MPPT structure

As per the given structure the final duty ratio ( $D_{wt}$ ) is addition of two duty ratio factors  $D_{eq}$  and  $D_{smc}$  which are generated by multiple variables. The final duty ratio ( $D_{wt}$ ) is given as:

$$D_{wt} = D_{eq} + D_{smc} \quad (1)$$

$$D_{eq} = 1 - \left[ \frac{v_{in}}{v_{out}} \right] \quad (2)$$

$$D_{smc} = \frac{k}{2} (1 + \varepsilon + \text{sat}(\sigma, \varphi)) \quad (3)$$

As per expression (2) and (3)  $v_{wt}$  and  $v_{out}$  are the input and output voltages of the AC/DC boost converter. These variables determine the duty factor  $D_{eq}$ , where as the  $D_{wt}$  duty factor is determined by variables 'k' and 'ε' which are controller gain and error coefficient respectively [10]. The  $\text{sat}(\sigma, \varphi)$  is determined as:

$$\text{sat}(\sigma, \varphi) = \begin{cases} 1 & \text{if } \sigma > \varphi \\ \frac{\sigma}{\varphi} & \text{if } |\sigma| \leq \varphi \\ -1 & \text{if } \sigma < -\varphi \end{cases} \quad (4)$$

Here,  $\varphi$  is the sliding layer value considered between -0.5 to 0.5. And the  $\sigma$  is calculated as:

$$\sigma = v_{wt} + i_{mwt} \left( \frac{dv_{wt}}{di_{mwt}} \right) \quad (5)$$

Here,  $i_{mwt}$  is the estimated current at maximum power determined by classic P&O MPPT technique,  $dv_{wt}$  and  $di_{mwt}$  are the change in  $v_{wt}$  and  $i_{mwt}$ . The  $i_{mwt}$  value is calculated by the below comparative expression generated by P&O MPPT technique.

$$i_{mwt} = i_{mwt}(t-1) + \nabla D_{wt} \left\{ \begin{array}{l} \text{If } P(t) > P(t-1) \text{ and } V(t) > V(t-1) \\ \text{If } P(t) < P(t-1) \text{ and } V(t) < V(t-1) \end{array} \right\} \quad (6)$$

$$i_{mwt} = i_{mwt}(t-1) - \nabla D_{wt} \left\{ \begin{array}{l} \text{If } P(t) < P(t-1) \text{ and } V(t) > V(t-1) \\ \text{If } P(t) > P(t-1) \text{ and } V(t) < V(t-1) \end{array} \right\} \quad (7)$$

Here,  $i_{mwt}(t-1)$  is the previous value of  $i_{mwt}$ ,  $\nabla D_{wt}$  is the updated variable to the  $i_{mwt}$  either increasing or decrease as per conditions.  $V(t)$ ,  $P(t)$  and  $V(t-1)$ ,  $P(t-1)$  are the present and past values of input voltage and power to the boost converter

respectively [11]. The final duty ratio ( $D_{wt}$ ) generated by these expressions is compared to high frequency triangular waveform generating PWM pulse for IGBT boost converter switch. The maximum power extraction is achieved with sliding control of the duty ratio and the power is fed to DC link. Each converter of the renewable source has individual SMC P&O MPPT technique integrated in each module.

## V. Active Power Control Based Anti-Windup Proportional Integral (APC Based Anti-Windup PI Controller)

The APC-based AWPI controller is an advanced approach for managing the interfacing inverter between the load and the DC link. This controller requires feedback from load voltage and current signals to maintain a stable voltage magnitude and frequency [12]. Figure 4 illustrates the overall control framework of the proposed APC-based AWPI controller, which employs a Sinusoidal PWM technique.

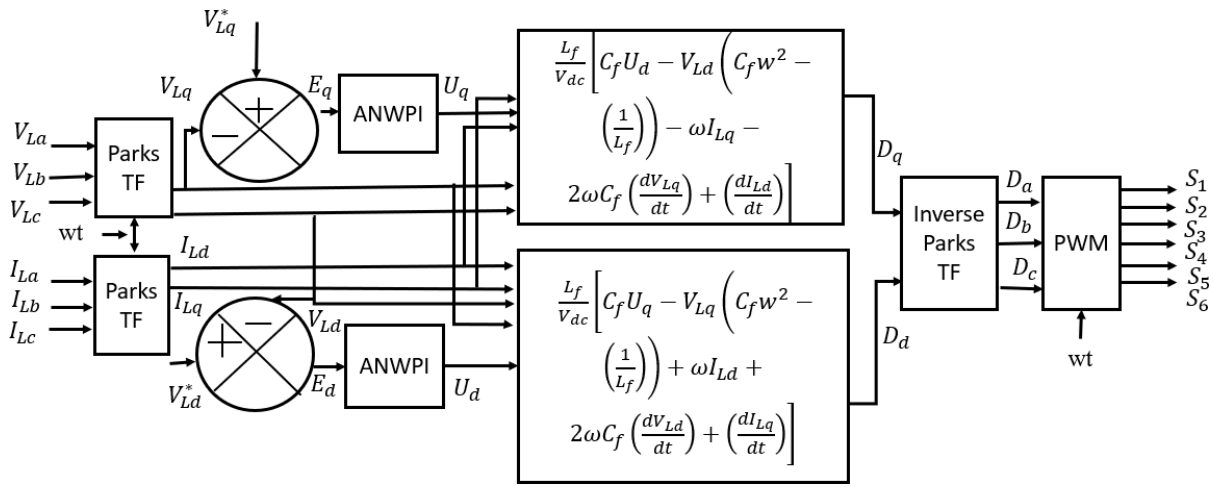


Figure 4: APC base AWPI controller of interfacing inverter module

The reference signals for the Sinusoidal PWM generator are derived from the dq components ( $D_d$  and  $D_q$ ). The controller relies on the dq components of the load voltages and currents to generate these reference signals. The dq components of  $V_{Labc}$  and  $I_{Labc}$  are computed using Park's transformation, as shown in the following equation:

$$\begin{bmatrix} f_d \\ f_q \end{bmatrix} = \begin{bmatrix} \sin \theta & -\cos \theta & 0 \\ \cos \theta & \sin \theta & 0 \end{bmatrix} \begin{bmatrix} f_a \\ f_b \\ f_c \end{bmatrix} \quad (8)$$

Here, 'f' can be any signal either VL or IL and ' $\theta$ ' is the phase angle of phase A determined by PLL (Phase Lock Loop) block [13]. The PLL is fixed with 50Hz fundamental frequency for the operation of the inverter at specified frequency. From the VL and IL dq components achieved from expression (6) the reference signals  $d_d$  and  $d_q$  are generated as:

$$D_d = \frac{L_f}{V_{dc}} \left[ C_f U_d - V_{Ld} \left( C_f \omega^2 - \left( \frac{1}{L_f} \right) \right) - \omega I_{Lq} - 2\omega C_f \left( \frac{dV_{Lq}}{dt} \right) + \left( \frac{dI_{Ld}}{dt} \right) \right] \quad (9)$$

$$D_q = \frac{L_f}{V_{dc}} \left[ C_f U_q - V_{Lq} \left( C_f \omega^2 - \left( \frac{1}{L_f} \right) \right) + \omega I_{Ld} + 2\omega C_f \left( \frac{dV_{Ld}}{dt} \right) + \left( \frac{dI_{Lq}}{dt} \right) \right] \quad (10)$$

Here,  $V_{dc}$  is the measured DC link voltage,  $L_f$  and  $C_f$  are the filter inductance and capacitance values,  $\omega$  is the fixed angular frequency ( $2\pi \cdot 50$ ),  $\frac{dv_{Ld}}{dt}$  and  $\frac{dv_{Lq}}{dt}$  are the change in dq VL and IL values. The  $U_d$  and  $U_q$  components are generated using error Dq components fed to AWPI controller [14]. The  $U_d$  is generated by error component comparing  $V_{Ld}^*$  and  $V_{Ld}$ . Similarly,  $U_q$  is generated error component comparing  $v_{Lq}^*$  and  $V_{Lq}$ .

$$E_d = V_{Ld}^* - V_{Ld} \quad (11)$$

$$E_q = V_{Lq}^* - V_{Lq} \quad (12)$$

The internal modelling of the AWPI controller with input and output signals is presented in Figure 5.

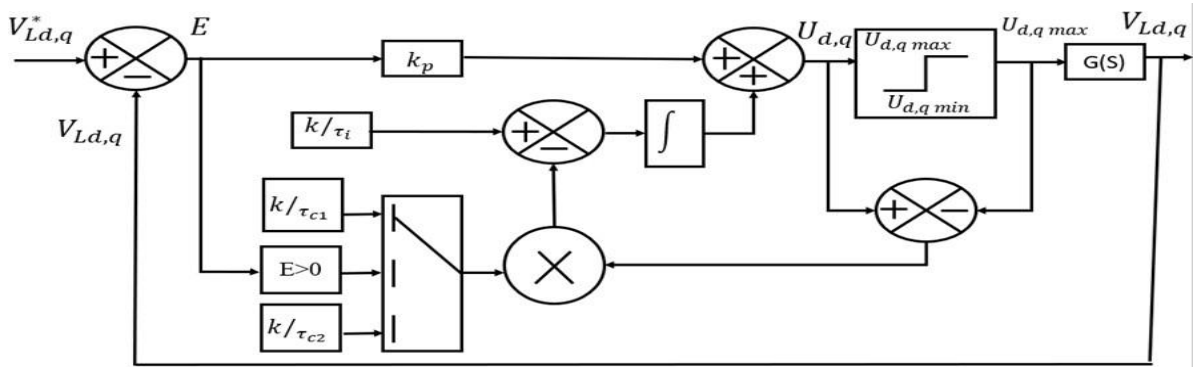


Figure 5: AWPI controller internal structure

Similar to conventional PI controller, the AWPI controller has fixed proportional gain ' $k$ '. The integral gain is varied as per the error signal ( $e$ ) of dq voltage components [14]. The  $u_d$  and  $u_q$  signals are given as:

$$U_d = E_d \left( \frac{k\tau_c(\tau_i s + 1)}{\tau_i(\tau_c s + 1)} \right) + U_{d \max} \left( \frac{1}{(\tau_c s + 1)} \right) \quad (13)$$

$$U_q = E_q \left( \frac{k\tau_c(\tau_i s + 1)}{\tau_i(\tau_c s + 1)} \right) + U_{q \max} \left( \frac{1}{(\tau_c s + 1)} \right) \quad (14)$$

Where,  $\tau_i$  and  $\tau_c$  are the integral gain coefficients which are tuned as per the response of the system[15].

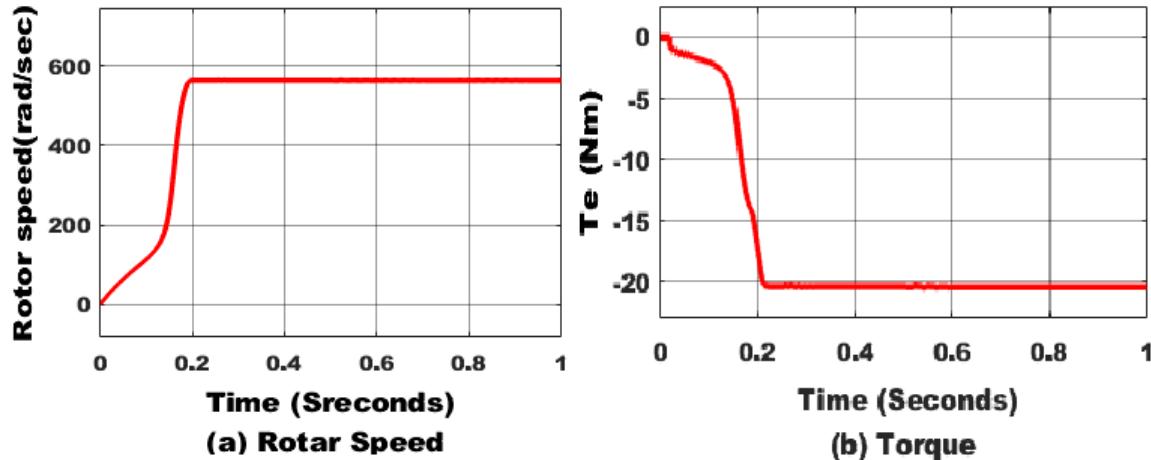
## VI. Results

The standalone renewable energy system, which includes a Battery Energy Storage (BES) module for load compensation, is modeled using Simulink. The simulation utilizes components from the 'Specialized Power Systems' library, incorporating elements from 'Electrical Sources,' 'Passive Elements,' 'Power Electronics,' and 'Commonly Used Blocks.' The parameters of each module are set according to the configuration values in Table 1, and the system is tested under various operating conditions.

Table 1: Configuration values of modules

Name of the module	Parameters
Wind module	PMBLDCG: 560Vdc, 35.17Nm, 3000rpm $R_s = 0.06\Omega$ , $L_s = 0.525\text{mH}$ , $\Phi = 0.1119\text{V.s}$ , $J = 0.0022\text{kg.m}^2$ , $F = 0.000425\text{N.m.s}$ , $p = 4$ Boost converter: $C_{in} = 1000\mu\text{F}$ , $L_b = 1\text{mH}$ , $R_{igbt} = 0.01\Omega$ , $V_{f\text{ diode}} = 0.8\text{V}$
Battery	Lithium Ion 70kWhr: $V_{nom} = 760\text{V}$ , Capacity = 100Ah,
Inverter	$R_{igbt} = 1\text{m}\Omega$ , $L_f = 1\text{mH}$ , $C_f = 100\mu\text{F}$
SMC MPPT	$\Delta D = \pm 1$ , MPPT gain = 5, $k = 0.017$ , $e = 0.05$ , $\varphi = -0.5$ , $f_s = 5\text{kHz}$
Active power control	$V_{Ld}^* = 240\text{Vrms ph}$ , $V_{Lq}^* = 0$ , $F_n = 50\text{Hz}$ , $k = 10$ , $r_i = 0.01$ , $r_{c1} = 0.1$ , $r_{c2} = 10$ , $f_s = 5\text{kHz}$

The standalone renewable energy system is updated based on the parameters provided in Table 1. The values for passive circuit elements and controller gains are determined through stability tuning. After updating these parameters, the simulation is performed using discrete analysis with the 'Tustin' solver in the 'powergui' block to generate graphical outputs. Voltage, power, and current waveforms for each module are plotted against simulation time, as presented below.



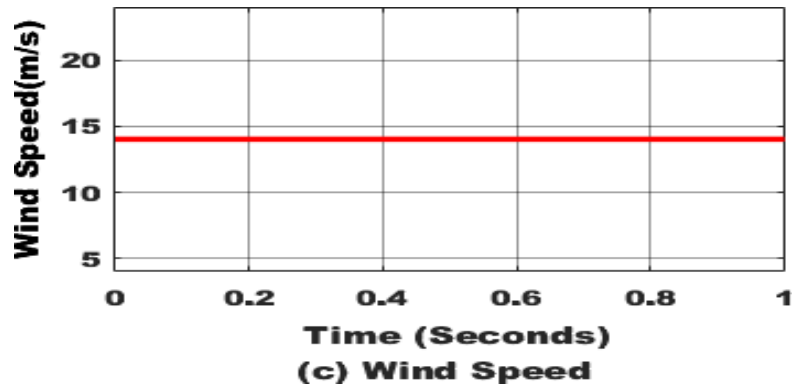


Figure 6: PMBLDCG characteristics.

From the Figure 6 PMBLDC generator in a wind energy system shows smooth acceleration, reaching a steady 560 rad/sec within 0.2 seconds, indicating effective control. The torque stabilizes at -22 Nm, confirming generator operation. With a constant 14 m/s wind speed, the system maintains stable performance, generating 12.3 kW of electrical power, demonstrating efficient wind energy conversion.

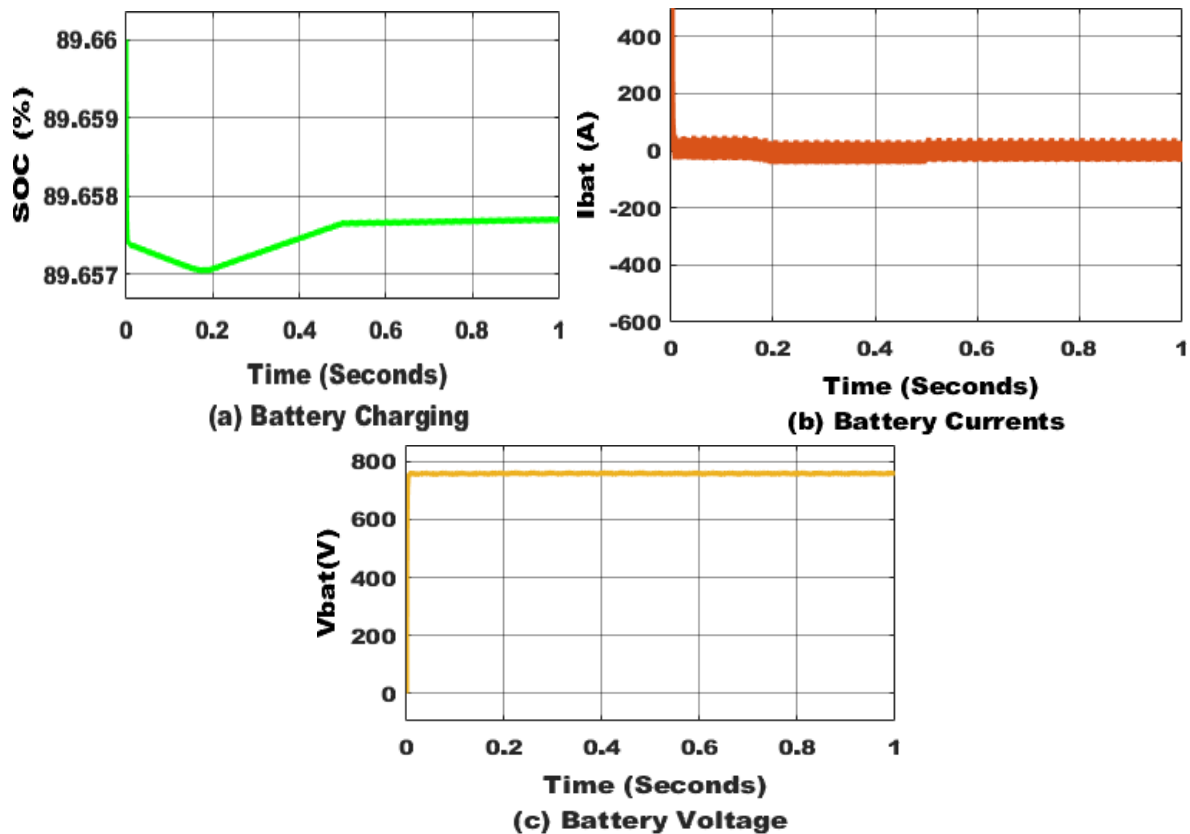


Figure 7: Battery pack characteristics

The battery pack at the DC link stores surplus power after meeting the load demand. As shown in Figure 7, the increase in State of Charge (SOC) and negative current signify the charging process from the renewable source. The recorded battery voltage is 760V, aligning with its nominal level at 90% initial SOC, ensuring effective energy storage.

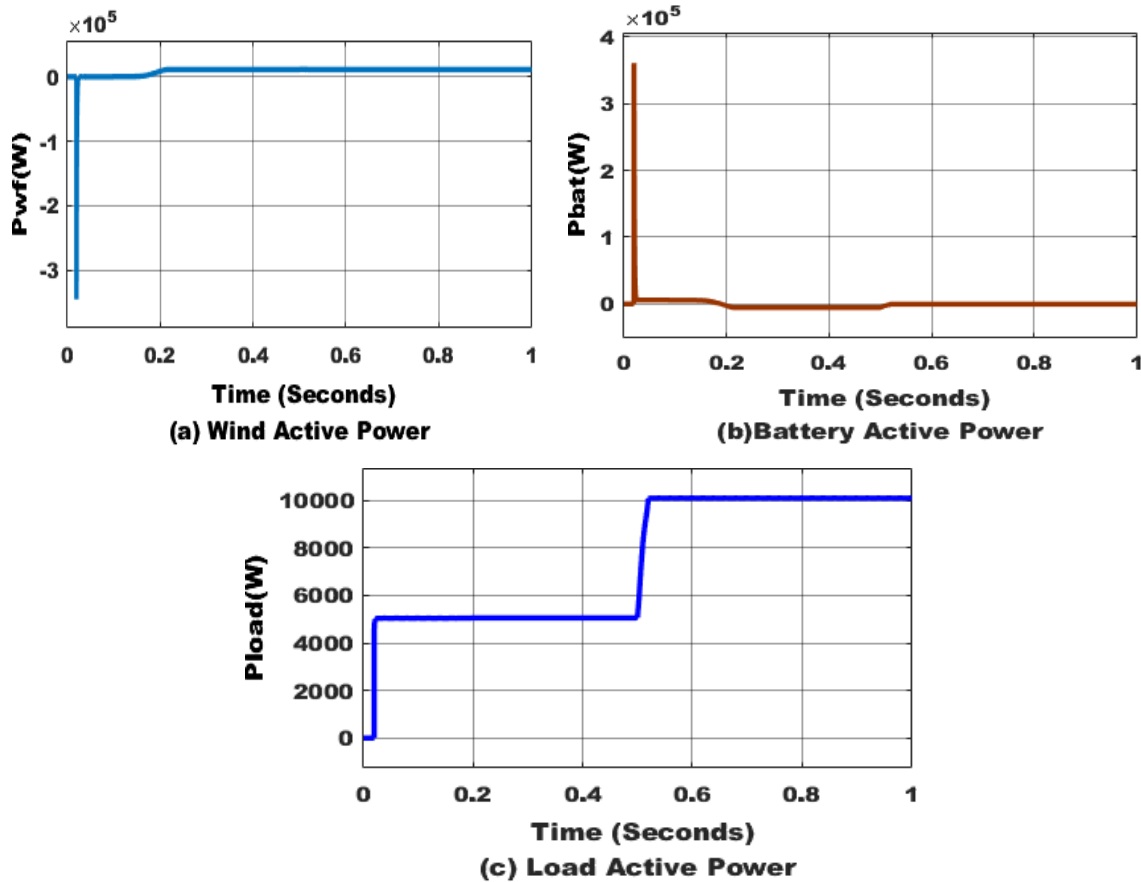


Figure 8: Active powers of wind, battery and load

From the Figure 8 Initially, the power demand rises sharply and stabilizes at around 5000 W. At approximately 0.5 seconds, there is another step increase, bringing the load power to 10,000 W, where it remains steady. The stepwise nature of the graph indicates sudden changes in load demand, which the system successfully accommodates, ensuring stable power supply. The active powers of the battery pack, wind generator and load demand. After the consumption of 10kW by the load the remaining renewable power of 1.5kW stored in the battery pack represented in negative direction.

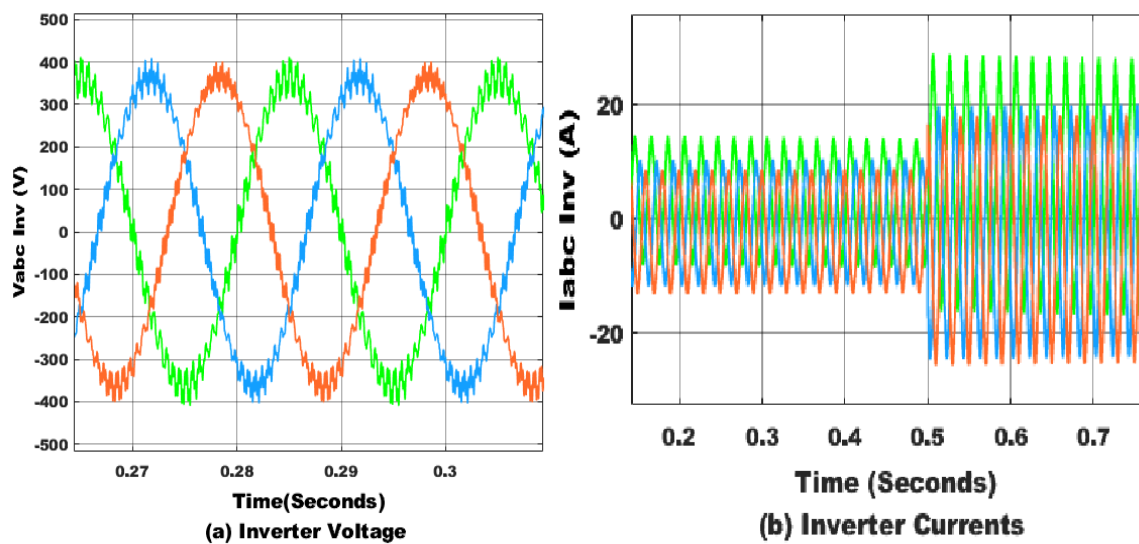


Figure 9: voltages and currents of Interfacing inverter

This analysis highlights the performance of a three-phase inverter by examining its output voltage, current, and power characteristics. The inverter produces balanced sinusoidal voltage waveforms with a  $120^\circ$  phase shift, maintaining a stable magnitude of  $\pm 400\text{V}$ . High-frequency switching ripples indicate the use of Pulse Width Modulation (PWM) for voltage regulation and improved power quality. Similarly, the current waveforms remain balanced, adapting to load variations, as evident from the amplitude rise around 0.5 seconds. After passing through an LC filter, the three-phase voltages and currents are measured, allowing the calculation of active and reactive power delivered by the inverter. These characteristics confirm the inverter's stable operation under varying load conditions.

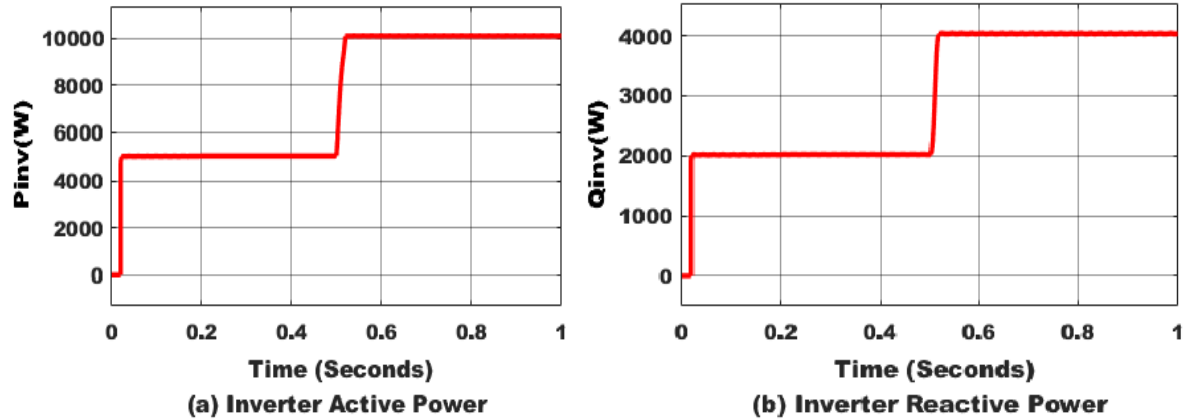


Figure 10: Interfacing inverter active (P) and reactive (Q) powers

The graphs illustrate the variations in the inverter's active and reactive power over time. The active power rapidly increases around 5000W and remains stable until 0.5 seconds, where it rises sharply to 10,000W, indicating a change in load. Similarly, the reactive power initially reaches 2000W, holding steady before increasing to 4000W at the same time mark, likely due to system adjustments. The consistent power levels before and after these changes demonstrate the inverter's capability to adapt to varying load conditions while maintaining stable operation. The wind generator power is extracted 11.3kW as plotted in Figure 8. the THDs (Total Harmonic Distortions) of the inverter voltage and current are calculated using FFT analysis tool and are presented in Figure 11.

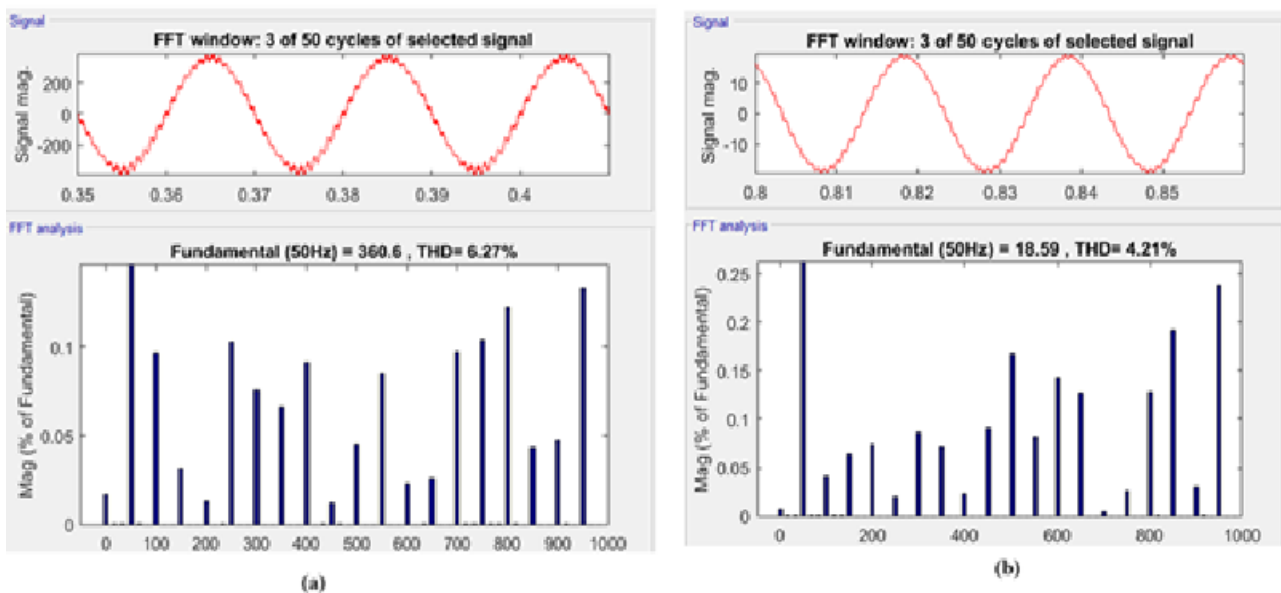


Figure 11: FFT analysis of a) Inverter Current and b) Inverter Voltage with AWPI controller

As per the calculated THDs of the voltage and current with SMC P&O MPPT the values are lower as observed in Figure 11.

## VII. Conclusion

A standalone renewable energy system with a battery energy storage (BES) module is developed using advanced MPPT techniques and an APC-based AWPI inverter control. The wind generator operates with power extraction converters regulated by SMC P&O MPPT, ensuring stable voltage and optimal power utilization. The generated power is either stored in the battery or supplied to the load as needed. Additionally, the AWPI control helps minimize **total harmonic distortion (THD)** in the three-phase inverter **voltage and current**. Further improvements in THD reduction can be achieved by integrating advanced control methods into the inverter's active power management.

## References

[1]. Rahman Habib, H. U., Wang, S., & Aziz, M. T. (2019). PV-Wind-Battery Based Standalone Microgrid System with MPPT for Green and Sustainable Future. 2019 9th International Conference on Power and Energy Systems.

(ICPES). doi:10.1109/icpes47639.2019.9105395.

[2]. Mohod, S. W., Hatwar, S. M., & Aware, M. V. (2011). Grid Support with Variable Speed Wind Energy System and Battery Storage for Power Quality. Energy Procedia, 12, 1032–1041. doi:10.1016/j.egypro.2011.10.135.

[3]. S. M. Mueen, R. Takahashi, and J. Tamura, "Operation and control of wind energy conversion systems," *IEEE Transactions on Sustainable Energy*, vol. 2, no. 4, pp. 389–398, Oct. 2011, doi: [10.1109/TSTE.2011.2158225](https://doi.org/10.1109/TSTE.2011.2158225).

[4]. J. F. Manwell, J. G. McGowan, and A. L. Rogers, *Wind Energy Explained: Theory, Design and Application*, 2nd ed. Wiley, 2009.

[5]. M. A. Hossain and H. R. Pota, "Robust Control for Power Sharing in Microgrids With Low-Inertia Wind and PV Generators," *IEEE Trans. Sustain. Energy*, vol. 6, no. 3, pp. 1067–1077, July 2015. DOI: [10.1109/TSTE.2015.2418339](https://doi.org/10.1109/TSTE.2015.2418339).

[6]. Lim, S.-C., Kim, M., Kang, J., & Lee, Y.-L. (2020). Subsampled Sum-Modified-Laplacian for Adaptive Loop Filter in Versatile Video Coding. *IEEE Access*, 8, 176330–176342. doi:10.1109/access.2020.3026649.

[7]. Elgendy, M. A., Zahawi, B., & Atkinson, D. J. (2012). Assessment of Perturb and Observe MPPT Algorithm Implementation Techniques for PV Pumping Applications. *IEEE Transactions on Sustainable Energy*, 3(1), 21–33. doi:10.1109/tste.2011.2168245.

[8]. Singh, B., & Sharma, S. (2012). "PMBLDCG based stand-alone wind energy conversion system for small scale applications." *International Journal of Engineering, Science and Technology*, 4(1), 65–73.

[9]. Kumar, R., & Chauhan, Y. K. (2014). "Permanent magnet brushless DC generator based stand-alone wind energy conversion system." *International Journal of Electrical and Computer Engineering*, 4(6), 858–865. DOI: [10.11591/ijece.v4i6.7057](https://doi.org/10.11591/ijece.v4i6.7057).

[10]. Kumar, D., & Chatterjee, K. (2016). A review of conventional and advanced MPPT algorithms for wind energy systems. *Renewable and Sustainable Energy Reviews*, 55, 957–970. doi:10.1016/j.rser.2015.11.013.

[11]. Sinha, S., & Chandel, S. S. (2014). "Review of software tools for hybrid renewable energy systems." *Renewable and Sustainable Energy Reviews*, 32, 192–205. DOI: [10.1016/j.rser.2014.01.035](https://doi.org/10.1016/j.rser.2014.01.035).

[12]. Femia, N., Petrone, G., Spagnuolo, G., & Vitelli, M. (2005). Optimization of Perturb and Observe Maximum Power Point Tracking Method. *IEEE Transactions on Power Electronics*, 20(4), 963–973. doi:10.1109/tpe1.2005.850975.

[13]. Liserre, M., Blaabjerg, F., & Hansen, S. (2005). Design and Control of an LCL-Filter-Based Three-Phase Active Rectifier. *IEEE Transactions on Industry Applications*, 41(5), 1281–1291. doi:10.1109/tia.2005.853373.

[14]. Peng, Y., Vrančić, D., & Hanus, R. (1996). A Review of Anti-Windup, Bumpless and Conditioned Transfer. *IFAC Proceedings Volumes*, 29(1), 1524–1529. doi:10.1016/s1474-6670(17)57883-0

[15]. A. Shishkin, A. Koulakov, J. Lillacci, and M. Khammash, "Anti-windup strategies for biomolecular control systems facilitated by model reduction," *Science Advances*, vol. 9, no. 10, pp. 1–12, Mar. 2023. doi: [10.1126/sciadv.adl5439](https://doi.org/10.1126/sciadv.adl5439).





